Table of content

1.- Experimental section

Preparation of samples – The synthesis of maleimides was carried out as reported previously.[1] For the samples measured under ambient conditions, the reaction took place for 24 hours. The samples were immersed in 1 mM and 0.2 mM solutions in acetonitrile for Bn-mal and TPP-mal, respectively. After the 24 hours exposure, the samples were thoroughly rinsed with acetonitrile and dried under argon atmosphere for further characterization. Some experiments were performed by adding a base to the incubation solution (3 drops Et_3N). For UHV experiments, the exposure of the maleimides was carried out using commercial molecules purified by sublimation, the molecules were placed in a glass bulb that is connected to the ultra-high vacuum system by a leak valve that allows a precise control of the partial pressure of molecules in the vacuum system. The molecules in the glass bulb are in solid phase in equilibrium with their vapor pressure.

Atomic Force Microscopy (AFM) and Scanning-Tunnelling Microscopy (STM) at the liquid-solid interface – AFM measurements on the modified substrates were performed on a Cypher ES (Asylum Research) system at 32 °C. All topography measurements were performed in the air tapping mode using OMCL-AC240TS-R3 probes with a spring constant ~2 N/m and a resonance frequency ~70 kHz. The same tip was used to scratch away the organic film in the contact mode at a constant force of 100 nN to evaluate the layer thickness. STM and AFM data analysis was performed using WSxM 2.61.[2] STM experiments were performed at room temperature using a PicoLE (Keysight) STM system operating in constant-current mode. Imaging parameters were set at Vbias = - 1.2 V for the sample bias and Iset = 0.05 nA for the tunnelling current. STM tips were prepared by mechanical cutting from Pt/Ir wire (80%/20%, diameter 0.25 mm). STM measurements performed at liquid-solid interface were carried out using 1-phenyloctane as solvent.

Raman spectroscopy – Raman spectra were collected with a confocal Raman microscope (Monovista CRS+, S&I GmbH) using a 632.8 nm He–Ne laser directed on the surface through an objective (OLYMPUS, BX43 100×, N.A. 0.7) with an power of around 4.7 mW. The Raman scattering was collected using the same objective and guided to a Raman spectrograph (S&I GmbH) equipped with a cooled-charge coupled device (CCD) camera operated at –100 °C (Andor Technology, DU920P-BX2DD). The spectra were recorded as single point spectra in three different locations. All the measurements were carried out under ambient conditions at room temperature.

Ultra-high vacuum low temperature scanning tunnelling microscope

All experiments have been carried out in an ultra-high vacuum (UHV) chamber with a base pressure of 5×10^{-11} mbar equipped with a Joule Thompson STM (JT-STM) and facilities for tip and sample preparation. All STM data were measured with tip and sample thermalized at 1.2 K. In the case of our experimental setup the tunnelling voltage is applied always to the sample.

2.- Supplementary AFM images
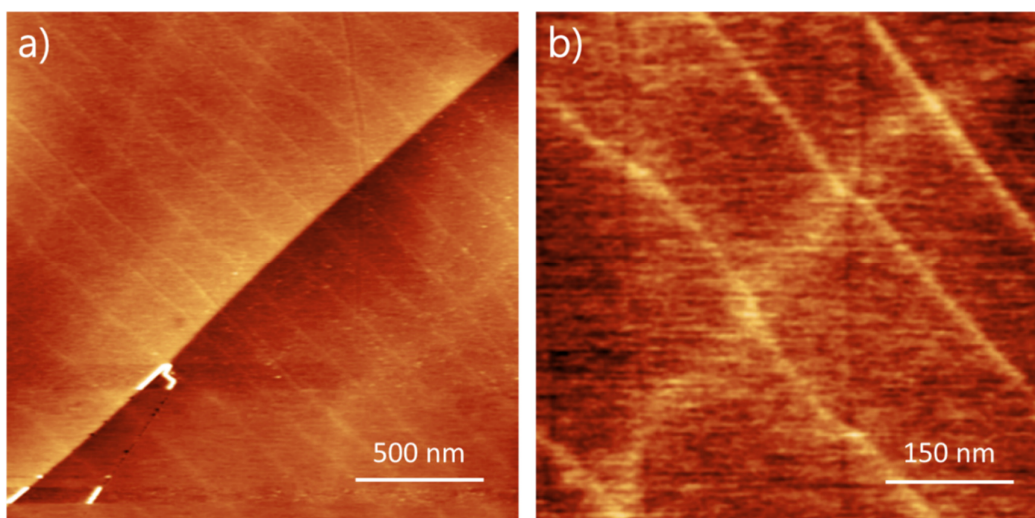
Fig. S1. AFM images of a) 2 μm x 2 μm and b) 0.6 μm x 0.6 μm for a bare surface of MoS_2.
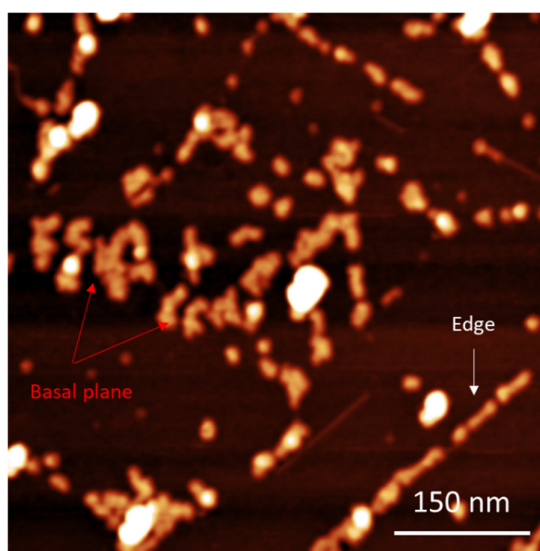
Fig. S2. AFM images of 0.6 μm x 0.6 μm for a Bn-succ-MoS_2 sample.
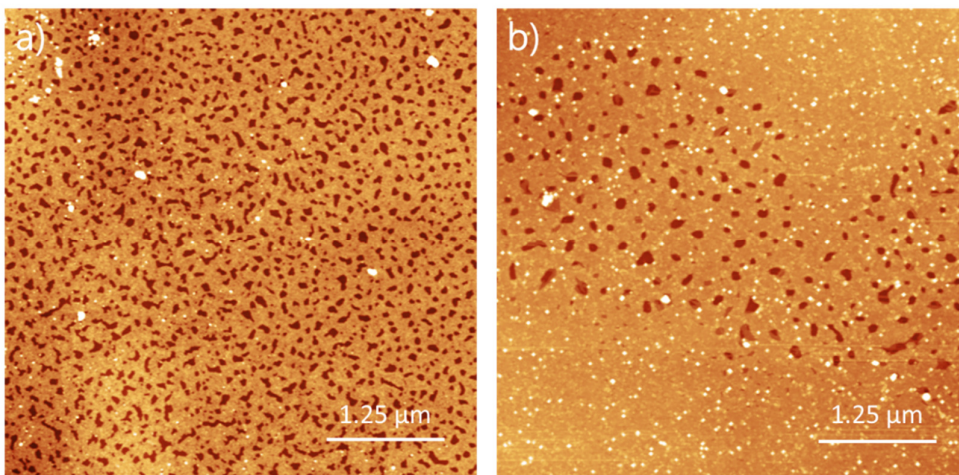
Fig. S3. AFM images of a) 5 µm x 5 µm and b) 5 µm x 5 µm for a surface of MoS$_2$ modified in presence of a base with the Bn-mal and TPP-mal compound, respectively.
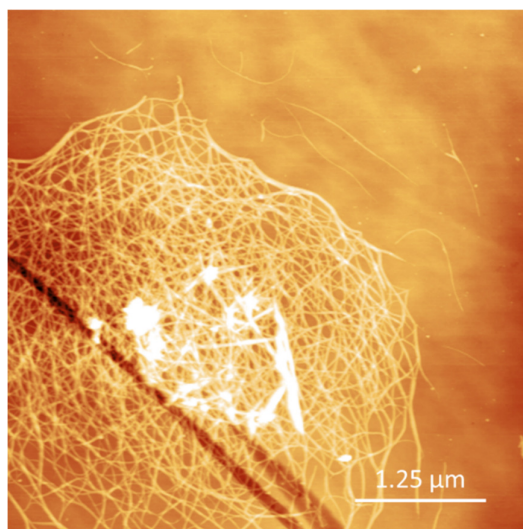
Fig. S4. AFM image of 5 µm x 5 µm for a surface of MoS$_2$ modified with the Bn-mal compound in presence of a base.

3.- UHV-STM images for clean MoS2 films

In order to grow the MoS_2 films we use graphene grown on Ir(111) as substrate. The interaction between graphene and Ir(111) is dominated by dispersion forces and the graphene overlayer behaves like self-standing graphene.[3]This characteristic make this surface ideal to study the properties of single molecules[4,5] or TMDs thin films[6]. The interaction between the MoS_2 overlayer and graphene is van der Waals and therefore the electronic and crystallographic properties of MoS_2 are expected to be unaltered[7]. The growth conditions in molecular beam epitaxy (MBE) of transition metal dichalcogenides on graphene have been extensively studied and it is possible to growth atomically thin layers with a high crystallographic perfection[6]. Figure S5(a) shows a scanning tunneling microscopy image with a lateral size of 200 nm showing the resulting islands after growth (see details in experimental methods). The islands are separated by clean graphene areas showing the moiré pattern between graphene and Ir(111), there are areas were sulphur is intercalated between graphene and Ir(111) but do not affect the growth of the MoS_2 overlayer. With the given growth conditions at this coverage the second layer is already observable in the middle of the MoS2 islands. Most of the islands present well defined straight edges forming 60 degrees to each other, a clear indication of the crystallinity of the islands further confirmed with atomically resolved images (see SI for further information).

Apart from the step edges there are two types of defects in the islands: atomic size defects in the middle of the terraces and linear defects going from one edge of the islands to another. These linear defects are common in TMDs films growth by MBE and are due to the coalescence of two MoS_2 islands that have nucleated at different points on the substrate and when they coalesce, the atomic lattices are not in registry. These defects are called mirror twin boundaries (MTB) and have been extensively studied[8,9]. The crystallinity of the MBE grown MoS_2 single layers is very high presenting a density of defects of the order of $2\times10^{-3} \pm 1\times10^{-3}$ defects per nm^2, approximately a defect every 6000 sulfur atoms.

Figure S5(b) shows an image measured using a negative sample bias voltage $V_b = -1.0$ V in which it is seen that both the edges of the islands and the defects appear brighter than the MoS_2 surface without defects. Figure S5c shows a STM image measured in the same area but with a positive bias voltage, $V_b = +1.8V$, applied to the sample. Contrary to what happen for the negative bias voltage at positive bias the defects look darker than the clean areas of the island. The difference in contrast in the STM images between the defects and the surface of the material can be rationalized considering that a monolayer of MoS_2 is a semiconductor with a direct gap of $1.29eV$[10], the presence of defects modifies locally the density of states[11–13]. The change in the contrast of the defects in the microscopy images allows us to identify clean defects present in the MoS_2 islands after the growth.
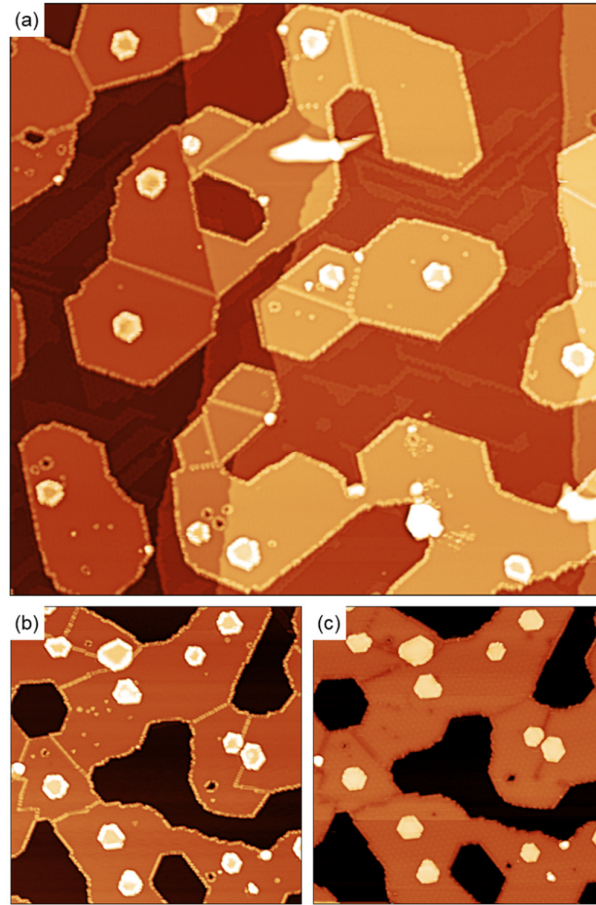
Fig. S5. STM images showing the resulting surface after growth. Most of the surface corresponds to the first monolayer of MoS_2 (orange tone), separated by graphene/Ir(111) (darker areas). There are small patches where the second layer has already started to grow (yellow tones). (a) Large scale image (200nm x 200nm, V_b = -1V, I_t = 10pA). Most of the MoS_2 islands present well-defined straight edges forming 60º to each other, a clear indication of the crystallinity of the film. Step edges and defects appear bright at negative bias voltages. STM images (130nm x130nm) measured at V_b = -1.0V (b) and V_b = +1.8V (c) on the same area. The defects on the MoS_2 film appear brighter than the MoS_2 terraces on the images acquired with negative bias voltages (b) and darker at negative bias voltage (c).

4.- Raman Spectroscopy
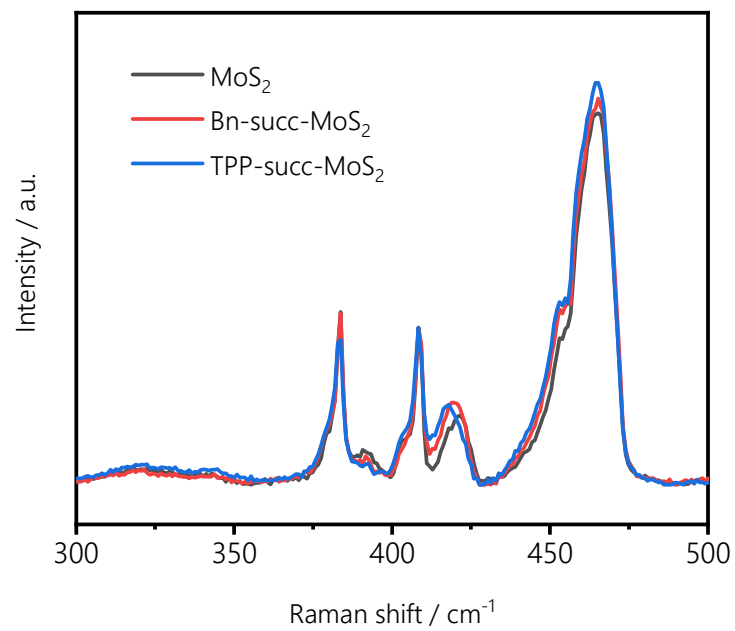
Fig. S6. Raman spectra for the bare substrate (black) and the samples prepared in absence of base (red and blue)

References

1   R. Quirós-Ovies, M. Vμzquez Sulleiro, M. Vera-Hidalgo, J. Prieto, I. JØnniferG ómez, V. Sebastıμn, J. antamaría and E. M. PØrez, , DOI:10.1002/chem.202000068.

2   I. Horcas, R. Fernández, J. M. Gómez-Rodríguez, J. Colchero, J. Gómez-Herrero and A. M. Baro, *Review of Scientific Instruments*, 2007, **78**, 18.

3   I. Pletikosić, M. Kralj, P. Pervan, R. Brako, J. Coraux, A. T. N'Diaye, C. Busse and T. Miⓩhely, *Phys Rev Lett*, 2009, **102**, 056808.

4   C. Díaz, F. Calleja, A. L. Vázquez de Parga and F. Martín, *Surf Sci Rep*, 2022, **77**, 100575.

5   S. Barja, M. Garnica, J. J. Hinarejos, A. L. Vázquez de Parga, N. Martín and R. Miranda, *Chemical Communications*, 2010, **46**, 8198.

6   J. Hall, B. Pielić, C. Murray, W. Jolie, T. Wekking, C. Busse, M. Kralj and T. Michely, *2d Mater*, 2018, **5**, 025005.

7   C. Murray, W. Jolie, J. A. Fischer, J. Hall, C. van Efferen, N. Ehlen, A. Grüneis, C. Busse and T. Michely, *Phys Rev B*, 2019, **99**, 115434.

8   M. Batzill, *Journal of Physics: Condensed Matter*, 2018, **30**, 493001.

9   H. Komsa and A. V. Krasheninnikov, *Adv Electron Mater*, , DOI:10.1002/aelm.201600468.

10   K. F. Mak, C. Lee, J. Hone, J. Shan and T. F. Heinz, *Phys Rev Lett*, 2010, **105**, 136805.

11   T. Verhagen, V. L. P. Guerra, G. Haider, M. Kalbac and J. Vejpravova, *Nanoscale*, 2020, **12**, 3019–3028.

12   J. Hong, Z. Hu, M. Probert, K. Li, D. Lv, X. Yang, L. Gu, N. Mao, Q. Feng, L. Xie, J. Zhang, D. Wu, Z. Zhang, C. Jin, W. Ji, X. Zhang, J. Yuan and Z. Zhang, *Nat Commun*, 2015, **6**, 6293.

13   W. Zhou, X. Zou, S. Najmaei, Z. Liu, Y. Shi, J. Kong, J. Lou, P. M. Ajayan, B. I. Yakobson and J.-C. Idrobo, *Nano Lett*, 2013, **13**, 2615–2622.